Thermoelectric properties of inorganic compounds

Igor Veremchuk[#], Michael Baitinger, Matej Bobnar, Felix Kaiser, Xinke Wang, Pawel Wyzga, Yuri Grin

The research on thermoelectric materials has drastically intensified over the last several decades. New paradigms, new concepts, new materials have been found. Common aspects include band convergence, "phonon-glass electron-crystal", multi-scale phonon scattering, resonance levels, anharmonicity, etc. Materials of ever higher ZT values have been reported. However, the origin of these high values are still disputed. From the chemical point of view, a better understanding of the relation between crystal chemistry, electronic structure and thermoelectric properties are expected to provide ways to improve the latter. The modern requirements of "green" energy technology boosts the search for new "friendly-for-environment" materials and their energy-conserving synthesis. Consequently, we focus our interest on the chemical insight of the well-known thermoelectric materials, and new ones, using also alternative synthesis routes.

Among the thermoelectric materials suitable for applications, PbTe-based compounds have an outstanding performance.

Pb – Eu – Te system [1].

The phases PbTe and EuTe crystallize both in the NaCl structure type, and it is commonly assumed that they form a solid solution over the entire concentration range $Pb_{1-x}Eu_xTe$. The lattice parameter of the $Pb_{1-x}Eu_xTe$ phase changes linearly with the composition for $x \leq 0.02$, and then remains unchanged (Fig.1). The slight reduction of the lattice parameter for the same composition after SPS is most probably caused by homogenization of the materials during spark-plasma treatment.

The electrical resistivity of samples $Pb_{1-x}Eu_xTe$ shows a bad-metal behavior in the temperature range below 500 K, and then changes to a semiconducting characteristic at higher temperatures (Fig. 2a), similar to the binary PbTe compound.

The Seebeck coefficient changes sign in the same temperature range indicating a *p–n* transition (Fig. 2b). The

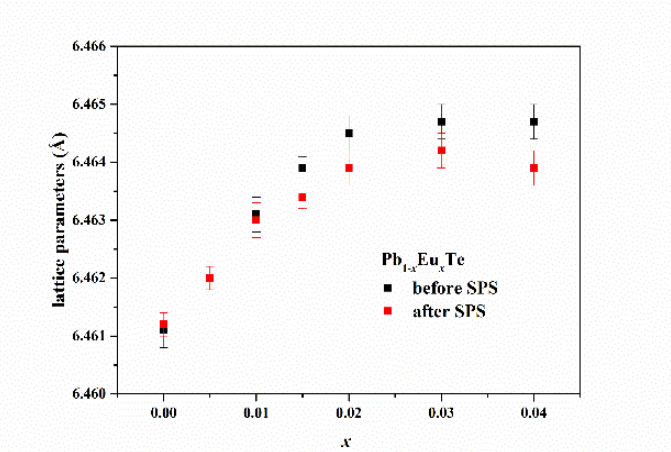

Fig.-1. Lattice parameters of $Pb_{1-x}Eu_xTe$ before (black) and after (red) SPS.

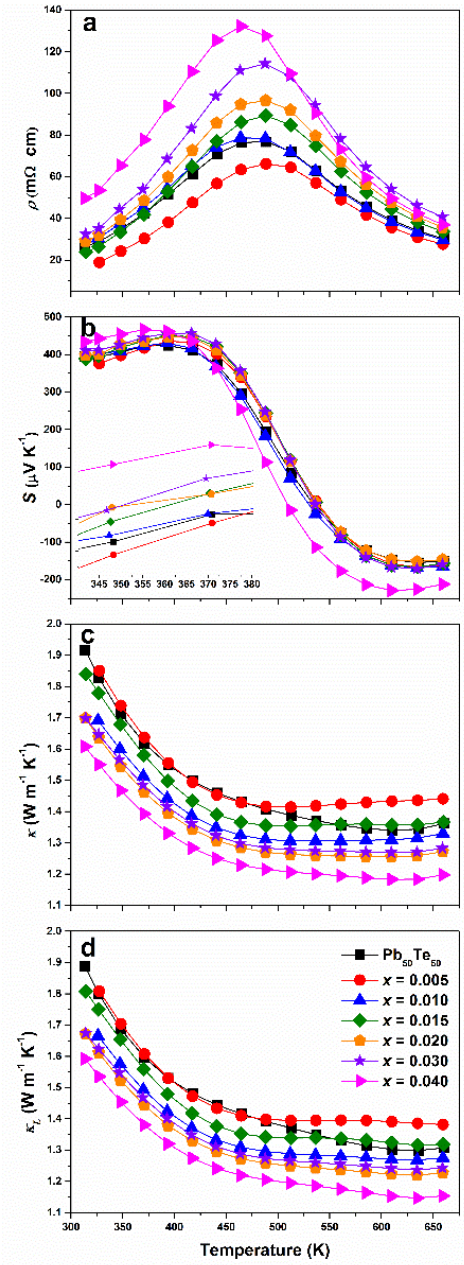

Fig.-2. Temperature dependence of thermoelectric properties of $Pb_{1-x}Eu_xTe$: electrical resistivity (a), Seebeck coefficient (b), total thermal conductivity (c), lattice thermal conductivity (d).

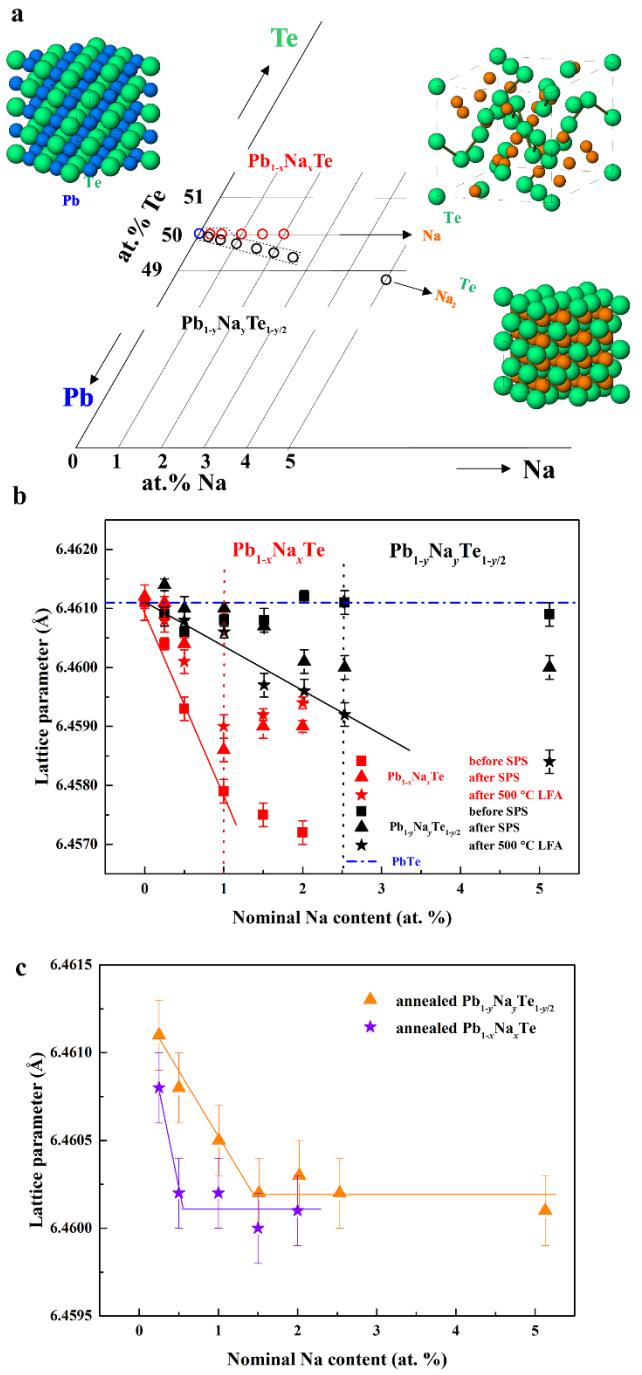

Fig.-3. (a) Compositions of the Na-substituted PbTe samples. (b) Lattice parameter vs nominal Na composition for the $Pb_{1-x}Na_xTe$ (red) and $Pb_{1-y}Na_yTe_{1-y/2}$ (black) series. (c) Lattice parameters of annealed Na-substituted PbTe samples.

thermal conductivity decreases with temperature below the *p–n* transition and remains practically unchanged above the transition (Fig. 2c and d). The values of the thermoelectric figure-of-merit, *ZT*, for $Pb_{1-x}Eu_xTe$ samples are in the same range and exhibit maximal values in the temperature range below the *p–n* transition due to the high Seebeck coefficient and the improved conductivity. As a results, lead-by-europium substitution does not influence the thermoelectric ability of stoichiometric lead telluride significantly.

Pb – Na – Te system [2].

The possibility of two substitution schemes is indicated (or assumed) by different Na additives (NaTe or Na_2Te) for the formation of acceptor centers. The known substitution scheme $Pb_{1-x}Na_xTe$ as well as a newly developed one $Pb_{1-y}Na_yTe_{1-y/2}$ were systemically investigated (Fig. 3a), and the shape of the solid solution of Na in PbTe in the ternary system Na – Pb – Te was established. Na has a limited, albeit different, solubility range for each series: 1.0 atom % for $Pb_{1-x}Na_xTe$, and 2.5 atom % for $Pb_{1-y}Na_yTe_{1-y/2}$ (Fig. 3b). The lattice parameters of the $Pb_{1-x}Na_xTe$ series decrease monotonically with increasing Na concentration up to 1 atom % (Figure 7b, red squares), a behavior in accord with the respective ionic radii of Na^{1+} (0.99 Å) and Pb^{2+} (1.19 Å). The relatively low limit of Na concentration can be understood considering the strong difference in the crystal structure: PbTe crystalizes in the ionic NaCl-type structure while Te polyanions are formed in NaTe (Fig. 3a). For the $Pb_{1-y}Na_yTe_{1-y/2}$ series ($y = 0.005-0.10$, Fig. 3a,b), the change of the lattice parameters with the substitution is not as strong as in the former case. This is conceivable assuming that the reduction of the lattice parameters due to the ionic radii of Pb^{2+} and Na^{1+} is partially compensated by the repulsive interaction of the cations around the Te defect. After annealing, the lattice parameters of both series obey Vegard's law, a trend, which is more prominent for the samples before annealing (Fig. 3c). After annealing the maximum solubility of Na is 1.5 atom % in the case of $Pb_{1-y}Na_yTe_{1-y/2}$ and 0.5 atom % for $Pb_{1-x}Na_xTe$, in contrast to 2.5 atom % and 1.0 atom %, respectively, before annealing. NMR can be understood assuming the clustering of the Na atoms around the Te defect (see report Bobnar). This suggestion is consistent with Crocker's idea about the formation of acceptor centers $Na_{Pb}\square_{Te}Na_{Pb}$ in PbTe and the formation of Na-rich nanosegregations or nanoscale precipitates. A long-term heat treatment leads to an equilibration and homogenization of the samples by reorganization and distribution of the Na clusters and Te vacancies. The thermoelectric properties of the single-phase materials were proven to be different for the different substitution schemes. The maximum *ZT* values of 1.4−1.6 at 760 K are established for both $Pb_{1-x}Na_xTe$ ($x \geq 0.02$) and $Pb_{1-y}Na_yTe_{1-y/2}$ ($0.1 \geq y \geq 0.03$) series in the multiphase samples due to the additional reduction

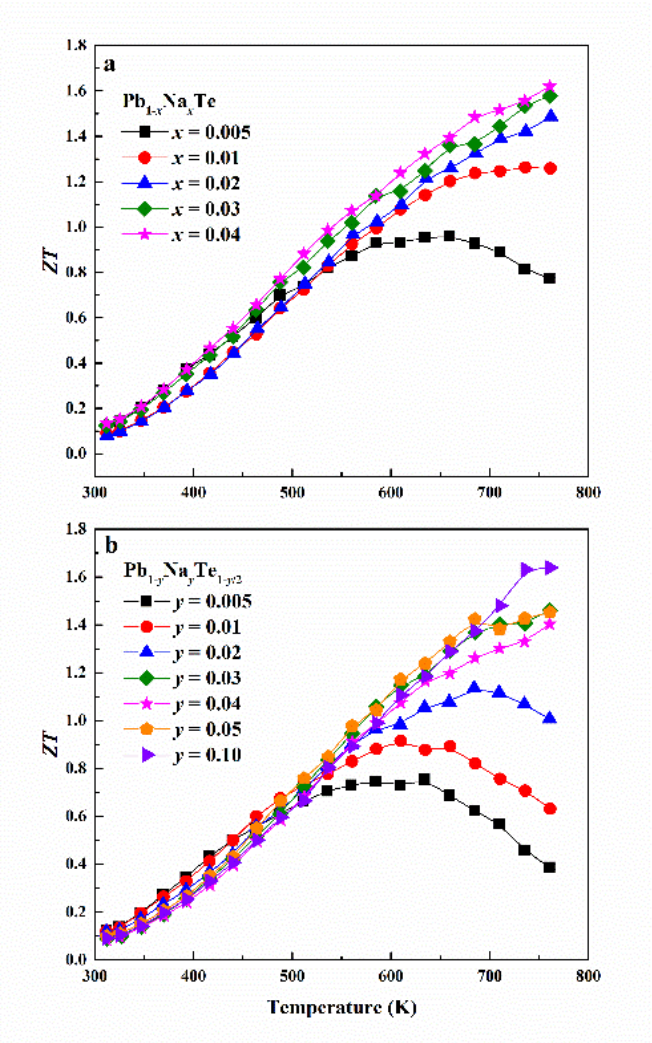

Fig.-4. Temperature dependences of the thermoelectric figure of merit ZT for (a) $Pb_{1-x}Na_xTe$ and (b) $Pb_{1-y}Na_yTe_{1-y/2}$.

of the thermal conductivity at the phase boundaries (Fig. 4).

Oxides [3,4].

An interesting approach is the exploitation of crystallographic shear (CS) for the reduction of the lattice thermal conductivity κ_{lat} due to increased phonon scattering. In the tungsten-oxygen system (Figure 5a) with decreasing O/W-ratio *x* the observed phases are the insulating ReO_3-type WO_3, the semiconducting phase $W_{20}O_{58}$ with CS planes, the metallic phase $W_{18}O_{49}$ with pentagonal columns (PC) and the metallic rutile-type WO_2 with varying coupling of the [WO_6] octahedra (Figure 5b–e). Such structure modifications result in an increasing charge carrier concentration. SPS combines the solid-state reaction of powdered precursor mixtures with simultaneous shaping, and provides an effective manufacturing route for materials due to low temperatures and short reaction times [5]. Thus, we studied the

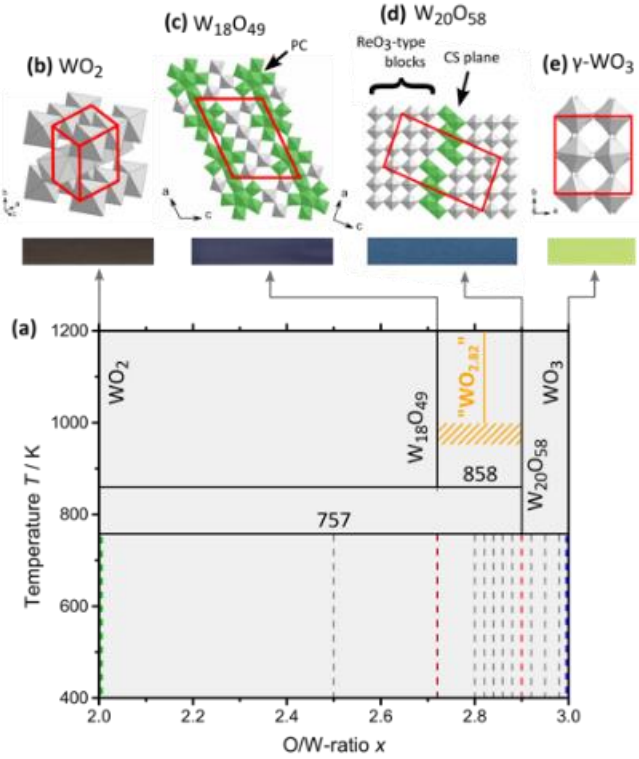

Fig.-5. (a) Phase diagram of the binary system W-O in the range of the O/W-ratio $2 \le x \le 3$. A metastable phase "$WO_{2.82}$" (orange) is found. (b–e) Crystal structures and respective colors of the known tungsten oxide phases.

products of the SPS redox reaction dependent on the composition *x* in the range $2.50 \le x \le 3$ (Figure 6a, dashed lines).

The solid-state reaction

$$x/3\ WO_3 + (1 - x/3)\ W \rightarrow WO_x \qquad (1)$$

was performed for different *x* by spark plasma sintering (SPS). Among the known phases, the lowest electrical conductivity $\sigma(T)$ values are measured for $WO_{2.90}$ with $77(3)\cdot10^3$ $S\cdot m^{-1}$ over the whole temperature range, which is at the level of a heavily doped semiconductor. The electrical conductivities of WO_2 and $WO_{2.72}$ indicate typical metallic behaviors with $\sigma(T) \propto 1/T$ dependency. Both metallic samples (WO_2 and $WO_{2.72}$) reveal a relatively high thermal conductivity $\kappa_{tot}(T) > 10$ $W\cdot m^{-1}\cdot K^{-1}$ (Figure 6a). However, in the dense WO_2 structure (Figure 6b), where strong tungsten–tungsten interactions are expected, this arises mainly from the lattice contribution κ_{lat}, whereas in $WO_{2.72}$ κ_{el} and κ_{lat} contribute equally (Figure 6b). For the electrically insulating WO_3 sample ($\kappa_{lat} = \kappa_{tot}$), the temperature dependence $\kappa_{lat}(T)$ appears to be similar to that of $WO_{2.72}$. $WO_{2.90}$ shows $\kappa_{tot} \approx 3.5$–4.5 $W\cdot m^{-1}\cdot K^{-1}$ over the whole temperature range (Figure 6a). Thus, the effect of CS planes in the $W_{20}O_{58}$ structure on the lattice thermal

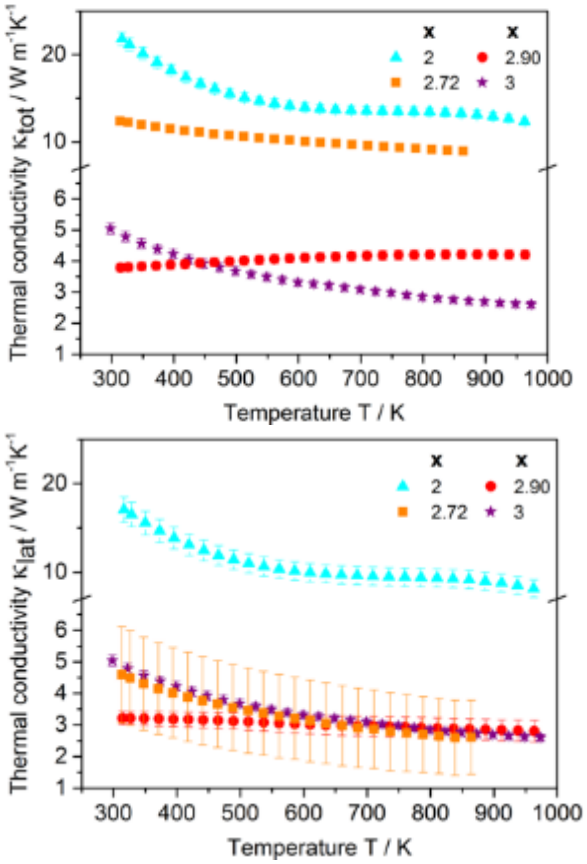

Fig.-6. Thermal conductivity of the oxides WO_2, $WO_{2.72}$, $WO_{2.90}$ and WO_3: (a) Total thermal conductivity κ_{tot}. (b) Lattice contribution $\kappa_{lat} = \kappa_{tot} - \kappa_{el}$

conductivity appears insignificant at high temperatures.

The figures of merit ZT at T = 860 K are only moderately high (0.006, 0.017 and 0.045 for WO_2, $WO_{2.72}$ and $WO_{2.90}$, respectively). A maximum ZT = 0.061 is found for $WO_{2.90}$ at 963 K.

Intermetallic clathrates [6].

Clathrate-I phases $K_8Li_xGe_{44-x/4}\square_{2-3x/4}$ ($0.25 < x < 2.7$), depending of the composition, show metal or semiconductor-like behavior with *n*-type conductivity. All samples have low thermal conductivities of 1 – 1.5 W m^{-1} K^{-1} at 300 K.

Outlook

On the first glance, the presented compounds adopt simple organizations of the atoms. All of them spark great interest in the field of thermoelectric materials. We showed that the seeming structural "simplicity" hides a great "complexity" on the atomic level. The latter has direct consequences for the improvement of the thermoelectric properties. This opens perspectives not only for the study of related compounds, but also for a wide range of new materials. Particularly, we would like to investigate the influence of structural 'imperfections' of the compounds on electrical and transport properties.

External Cooperation Partners

J.T. Zhao (Shanghai University, China; Texas Tech University, Lubbock, USA), W. Tremel (Mainz University, Germany); B. Kieback (Fraunhofer IFAM Dresden, Germany).

References

[1] *X. Wang, I. Veremchuk, M. Bobnar, J. T. Zhao and Y. Grin, Inorg. Chem. Frontiers* ***3*** *(2016) 1152.*
[2] *X. Wang, I. Veremchuk, M. Bobnar, U. Burkhardt, J. T. Zhao and Y. Grin, Chem. Of Mater.* ***30*** *(2018) 1362.*
[3] *G. Kieslich, G. Cerretti, I. Veremchuk, R.P. Hermann, M. Panthofer, Yu. Grin, W. Tremel. Physica Status Soliditi A – Applications and Mater. Sci.* ***213*** *(2016) 808.*
[4] *F. Kaiser, P. Simon, U. Burkhardt, B. Kieback, Y. Grin and I. Veremchuk, Crystals* ***7*** *(2017) 271.*
[5] *I. Veremchuk, I. Antonyshyn, C. Candolfi, X. Feng, U. Burkhardt, M. Baitinger, J.-T. Zhao and Y. Grin Inorg. Chem.* ***52*** *(2013) 4458.*
[6] *Y. Liang, W. Schnelle, I. Veremchuk, B. Böhme, M. Baitinger and Y. Grin, J. of Electronic Mater.* ***44*** *(2015) 4444.*

[#] Igor.Veremchuk@cpfs.mpg.de